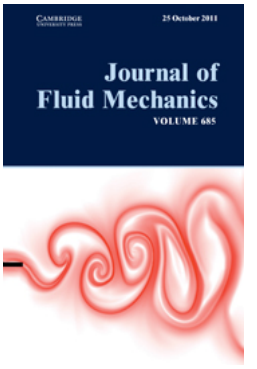

Do waveless ships exist? Results for single-cornered hulls

Philippe H. Trinh, S. Jonathan Chapman and Jean-Marc Vanden-Broeck

Journal of Fluid Mechanics / Volume 685 / October 2011, pp 413 - 439
DOI: 10.1017/jfm.2011.325, Published online: 06 October 2011

J. Fluid Mech. (2011), *vol.* 685, *pp.* 413–439.
doi:10.1017/jfm.2011.325

Do waveless ships exist? Results for single-cornered hulls

Philippe H. Trinh[1]†, **S. Jonathan Chapman**[2] **and Jean-Marc Vanden-Broeck**[3]

[1] PACM, Princeton University, Washington Road, Princeton, NJ 08544, USA

[2] OCIAM, Mathematical Institute, 24-29 St Giles', Oxford OX1 3LB, UK

[3] Department of Mathematics, University College London, Gower Street, London WC1E 6BT, UK

(Received 11 October 2010; revised 4 June 2011; accepted 26 July 2011)

Consider low-speed potential flow past a ship modelled as a semi-infinite two-dimensional body with constant draught. Is it possible to design the hull in such a way as to eliminate the waves produced downstream of the ship? In 1977, Vanden-Broeck & Tuck had conjectured that a single-cornered piecewise-linear hull will always generate a wake; in this paper, we show how recently developed tools in exponential asymptotics can be used to confirm this conjecture. In particular, we show how the formation of waves near a ship is a necessary consequence of singularities in the ship's geometry (or its analytic continuation). Comprehensive numerical computations confirm the analytical predictions.

Key words: surface gravity waves, wave–structure interactions

1. Introduction

The vast majority of the world's total trade is transported by sea-going ships. Ships produce waves and waves invariably represent a loss of energy, fuel, speed, and ultimately, money. So for the naval architect, the design of a (practically) waveless ship is of paramount importance, and indeed a great deal of numerical, experimental, and analytical research has been applied to this topic of ship optimization and wave resistance for over a century. Our interests, then, are simply stated: are waveless ships theoretically possible? If so, what restrictions must we placed on their design? If not, what can be done to minimise the production of waves?

Of course, when we refer to a waveless ship, we have a very specific regime in mind: that of potential flow (a standard assumption). Now in attempting to solve this problem, it becomes necessary to linearise the boundary conditions at the free surface, and as it concerns ship waves we generally have three ways of proceeding. The most standard and most well-developed method linearises the geometry of the ship by assuming that the hull is sufficiently small in one or several of its dimensions. For example, applying the thin-ship approximation leads to the well-known Mitchell integral, for which it has been shown that wave resistance can never vanish at any

† Email address for correspondence: ptrinh@princeton.edu

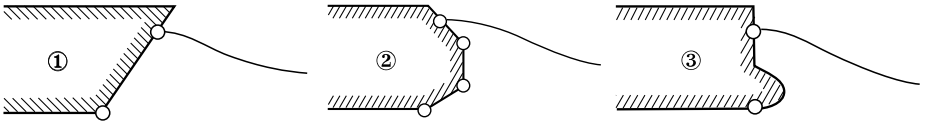

FIGURE 1. Can any of these hull forms be made waveless? ① is the single-cornered ship, ② is the multi-cornered ship, and ③ is the bulbous ship. The flow is from left to right, and nodes indicate singularities in the ship's geometry.

finite speed for ships of finite displacement (Kotik & Newman 1964 and Kostyukov 1968, p. 354). But as remarked by Tuck (1991*a*,*b*), one cannot be quite sure that a similar result will hold for non-thin ships.

Instead, if we wish to preserve the geometry of the ship in the approximation, an alternative linearisation can be performed by developing a solution valid as the Froude number tends to infinity. For these high-Froude-number problems, the flow detaches from the ship smoothly at leading order (zero gravity) and the free surface is a free streamline. Spurred on by the initial numerical computations of Vanden-Broeck (1980), Madurasinghe & Tuck (1986) would go on to discover waveless ships, an analysis which was later confirmed by the more detailed numerics of Farrow & Tuck (1995).

However, in discerning the effects of the ship's geometry on the resultant waves, the low-Froude-number limit is by far the more important and non-trivial choice. The reason is that the analysis near a blunt three-dimensional ship can be reduced to the study of the two-dimensional potential flow problem for which the ship is modelled as a semi-infinite body with constant draft (Dagan & Tulin 1972). Ultimately, it is the low-Froude limit which truly models the ship–water interactions and for which the nonlinearity of the ship's geometry is taken into account. Then, as an eventual goal, we would like to be able to recognise whether any of the three ships in figure 1 are waveless in the low-Froude-number limit. Note that in the potential flow problem, a waveless solution past the stern (rear) of a ship, could be equally used as a smoothly attaching ('splashless') bow flow. Thus, if the profiles in figure 1 are indeed solutions, then they are equally valid for flow in either direction.

There is an important difficulty. When an ideal fluid flows past a surface-piercing object or over an obstruction, waves are sometimes produced upstream or downstream of the disturbance. But in the low-speed limit, the traditional asymptotic series in powers of the Froude number fails to capture this phenomenon – this is the so-called *Low-Speed Paradox* first mentioned by Ogilvie (1968). The waves are in fact exponentially small (in the Froude number) and thus invisible to any traditional asymptotic analysis.

This formidable singular limit has been painfully problematic in regard to previous asymptotic and numerical treatments of the ship–wave problem. The fully nonlinear problem was first computed by Vanden-Broeck & Tuck (1977), and on the basis of numerical evidence, they conjectured that ship hulls with a single front face will always generate waves (see also Vanden-Broeck 1985, 2010, for further details and a review of these early results). Moreover, the earlier experimental work of Baba (1976) had indicated that a bulbous bow can eliminate, or at least reduce, the splash at the bow of a ship. This prompted the discovery of seemingly waveless ships with bulbous profiles, first by Tuck & Vanden-Broeck (1984) and later confirmed by Madurasinghe (1988) – but again, only numerically so. Another surprising result was suggested by Yeung (1991), whose more recent numerics suggested that, for the single-cornered hull, there exists a critical Froude number below which no trailing waves are possible – in

direct contrast to Vanden-Broeck & Tuck (1977). Unfortunately, these last three results were refuted by the more comprehensive numerical study of Farrow & Tuck (1995); there, they wrote:

> *The free surface would at first sight appear to be waveless, but on closer examination of the numerical data, there are very small waves present and they have a steepness of* 1.5×10^{-3},

a comment they had made in reference to the bulbous profiles studied in Tuck & Vanden-Broeck (1984). Clearly, these are questions which cannot be easily answered using simple numerics. Indeed, in *Reminiscences and Reflections: Ship Waves, 1950–2000*, Tulin mentions two open questions:

> *The fundamental questions of whether such rising potential free-surface flows before bluff bodies exist [...] still remain open*,

and

> *Is it demonstrable [...] that continuous solutions will not exist in the limit of vanishing speed? Does this have anything to do with the inability of Tuck and his colleagues [...] to find a continuous solution in the two-dimensional bow wave case? Do nonbreaking flows exist at all for surface-piercing ship forms of arbitrary form and thickness, at any speed?*

The key to resolving the Low-Speed Paradox is dependent on a clear understanding of asymptotic divergence – its causes and its consequences. The low-Froude-number limit is singular and causes the leading-order rigid-wall solution to exhibit singularities in its analytic continuation, which eventually produces the divergence of the series. This divergence, in turn, is associated with the presence of exponentially small corrections to the algebraic expansion – in this case, representing our hidden free-surface waves. And thus, the collection of tools to detect these corrections is often referred to as *exponential asymptotics* or *asymptotics beyond all orders* (see for example, reviews by Dingle 1973; Boyd 1998, 1999).

The resolution of the Low-Speed Paradox for the case of gravity waves over a submerged obstruction was given by Chapman & Vanden-Broeck (2006) (see also Chapman & Vanden-Broeck 2002, for a similar study of capillary waves). In this paper, we will extend Chapman & Vanden-Broeck's work to the problem of surface-piercing bodies, and in particular, we will derive an analytical expression for the waves produced by flow past a single-cornered ship. We will show how these exponentially small waves must arise when the solution crosses the Stokes line originating from the corner-singularity of the stern; in doing so, we thus confirm the 1977 conjecture of Vanden-Broeck & Tuck concerning the impossibility of waveless single-cornered ships. Finally, we provide sufficiently accurate numerical simulations which confirm our analytical predictions.

2. Mathematical formulation

Let us consider two-dimensional steady irrotational flow past a semi-infinite body, which consists of a flat bottom ($y = -H, x < 0$), and a face oriented at an angle $\pi\sigma$ to the horizontal ($0 < \sigma < 1$). There is a uniform stream of speed U as $x \to -\infty$, and we assume that the flow attaches to the stern at a stagnation point.

With $\phi(x, y)$ denoting the velocity potential, the problem can be non-dimensionalised so that: (i) the stagnation point is located at $(x, y) = (0, 0)$ and $\phi = 0$;

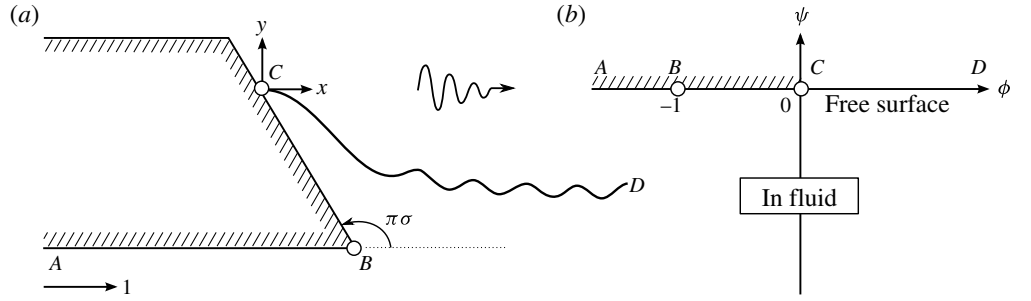

FIGURE 2. Non-dimensional flow past a one-cornered ship, shown in the physical xy-plane (a), and in the potential $w = \phi + \mathrm{i}\psi$ plane (b).

(ii) the corner of the stern is located at $\phi = -1$; and (iii) the potential tends to the unit free stream, $\phi \to 1$, as $x \to -\infty$. The motion of the fluid (see Vanden-Broeck 2010; Trinh 2010) is then governed by Laplace's equation, with the kinematic condition on all boundaries, and Bernoulli's equation on the free surface:

$$\nabla^2\phi = 0 \quad \text{for } (x, y) \text{ in the fluid,} \tag{2.1}$$

$$\frac{\partial\phi}{\partial n} = 0 \quad \text{for } (x, y) \text{ on the hull and free surface,} \tag{2.2}$$

$$\frac{\epsilon}{2}|\nabla\phi|^2 + y = 0 \quad \text{for } (x, y) \text{ on the free surface,} \tag{2.3}$$

where all variables now non-dimensional. The parameter $\epsilon = U^2/gL$ is related to the square of the draft-based Froude number and $\epsilon \ll 1$ is the low-Froude-number regime we shall study. Here, L is defined as the ratio of the dimensional value of the potential at the corner, divided by U. The physical and potential planes are shown in figure 2.

Unfortunately, formulated as a function of Cartesian coordinates (x, y), the problem is rather difficult to approach, especially since the dynamic condition (2.3) must be applied to an as-yet unknown free surface. In the simplifying hodograph formulation, we introduce the complex potential $w = \phi + \mathrm{i}\psi$ and let $z = x + \mathrm{i}y$. The ship/free surface is chosen to be the streamline $\psi = 0$ and now, both Laplace's equation (2.1) and the kinematic condition (2.2) are immediately satisfied, so long as we ensure the complex potential is analytic. We then define

$$q\mathrm{e}^{-\mathrm{i}\theta} \equiv \frac{\mathrm{d}w}{\mathrm{d}z} = u - \mathrm{i}v, \tag{2.4}$$

so q is the speed of the flow and θ is the angle the streamline makes with the x-axis. Differentiating Bernoulli's equation (2.3) tangentially, that is, with respect to ϕ, yields

$$\epsilon q^2 \frac{\mathrm{d}q}{\mathrm{d}\phi} + \sin\theta = 0, \tag{2.5}$$

where the free-surface condition is applied to the streamline $\psi = 0$ for $\phi > 0$. To close the system, we need one final equation, and this will be given by using the analyticity of the logarithm of the hodograph variable, $\log q - \mathrm{i}\theta = \log \mathrm{d}w/\mathrm{d}z$. By Cauchy's theorem, it can be shown that

$$\log q = \frac{1}{\pi}\int_{-\infty}^{\infty} \frac{\theta(\varphi)}{\varphi - \phi}\,\mathrm{d}\varphi, \tag{2.6}$$

which is the usual boundary integral result for two-dimensional free-surface flows. Imposing the hull geometry and setting $\theta = 0$ for $\phi < -1$ and $\theta = \pi\sigma$ for $-1 < \phi < 0$ then gives

$$\log q = \log\left(\frac{\phi}{\phi+1}\right)^{\sigma} + \frac{1}{\pi}\int_0^{\infty} \frac{\theta(\varphi)}{\varphi-\phi}\,\mathrm{d}\varphi. \tag{2.7}$$

Note that the relation between ϕ and the physical plane (and hence the physical size of the ship's face) can be determined *a posteriori* once (2.5) and (2.7) have been solved.

3. Complexification and the Stokes phenomenon

The general methodology of our ship–wave analysis can be described as follows: when the fluid speed, $q(\phi)$, and streamline angle, $\theta(\phi)$, are expressed as asymptotic expansions in powers of the Froude number, ϵ, we find that the approximations are waveless at every order. The free-surface waves produced by the ship's hull are, in fact, exponentially small and thus *beyond-all-orders* of the regular asymptotic expansions.

Of course, the velocity $q\mathrm{e}^{-\mathrm{i}\theta}$ is entirely well-behaved on the free surface ($\psi = 0$ and $\phi > 0$), but its analytic continuation contains a singularity at $\phi = -1$, which corresponds to the corner of the ship. To study this issue, we complexify the free surface, writing $\phi \mapsto \overline{\phi} + \mathrm{i}\overline{\psi} = \overline{w} \in \mathbb{C}$ and $q\mathrm{e}^{-\mathrm{i}\theta} \mapsto \overline{q}\mathrm{e}^{-\mathrm{i}\overline{\theta}} = \mathrm{d}\overline{w}/\mathrm{d}\overline{z} \in \mathbb{C}$. However, because of the nature of complex variables, we may continue to identify these new complexified variables $\overline{w}$ and $\mathrm{d}\overline{w}/\mathrm{d}\overline{z}$, with the usual quantities of w (the complex potential) and $\mathrm{d}w/\mathrm{d}z$ (the complex velocity). Thus, within this paper, we will often mention the 'corner of the ship', but we are referring to the singularity in the analytic continuation, which is identifiable with the corner, rather than the physical corner itself.

If we extend both the boundary integral (2.7) and the dynamic condition (2.5) into the upper or lower half-ϕ-plane, this yields

$$\log q \pm \mathrm{i}\theta = \log\left(\frac{w}{w+1}\right)^{\sigma} + \mathscr{H}[\theta(w)], \tag{3.1a}$$

$$\epsilon q^2 \frac{\mathrm{d}q}{\mathrm{d}w} + \sin\theta = 0, \tag{3.1b}$$

where we have replaced the complexified ϕ by w and the $\pm$ signs correspond to analytic continuation into the upper and lower half-ϕ-planes, respectively. We have also introduced the notation

$$\mathscr{H}[\theta(w)] = \frac{1}{\pi}\int_0^{\infty} \frac{\theta(\varphi)}{\varphi - w}\,\mathrm{d}\varphi, \tag{3.2}$$

to represent the Hilbert transform of θ, integrated over the free surface, $\varphi \geqslant 0$.

The singularity, seen in (3.1*a*), has two important consequences, both of which follow from the basic tenets of exponential asymptotics (see for example, reviews by Dingle 1973; Boyd 1998, 1999). First, it causes the expansions of q and θ to diverge for $w \in \mathbb{R}^+$. In order to achieve the best approximation, the expansions must then be *optimally truncated*, at which point the remainder is exponentially small. The second role of the singularity is to generate critical curves (*Stokes lines*) in the complex plane. When w is analytically continued across such curves, the exponentially small remainder 'switches-on' in a process known as the *Stokes Phenomenon*. As it relates to the ship–wave problem, this switching-on mechanism is illustrated in figure 3.

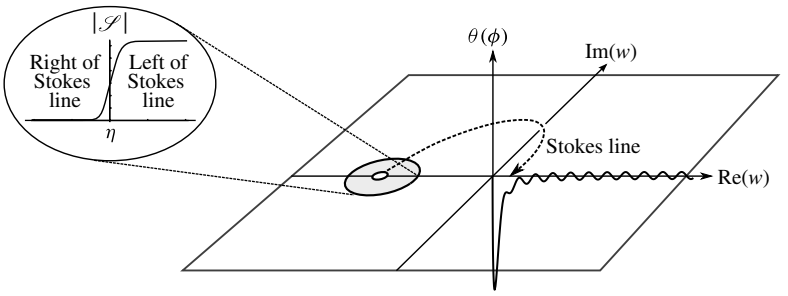

FIGURE 3. The physical solution in the ship–wave problem is $\theta(\phi)$ for $\phi \in \mathbb{R}^+$. For $\epsilon \to 0$, the asymptotic expansion for ϕ diverges because of the singularity in its analytic continuation (shown as a perpendicular plane, $\phi = w \in \mathbb{C}$). By re-scaling near the singularity and optimally truncating, we will be able to observe the smooth switching-on of the exponentially small terms, scaled by the Stokes switching parameter, $\mathscr{S}$.

4. Asymptotic approximation

We shall begin by performing the asymptotic analysis of (3.1*a*) and (3.1*b*) for analytic continuation into the upper half-w-plane. The final ship waves will also require the same analysis for continuation into the lower half-plane as well. The initial analysis is nearly identical to the one in Chapman & Vanden-Broeck (2006) for gravity waves over non-surface-piercing obstructions, but we include it here for completeness.

Substituting the usual perturbation expansion

$$\theta = \sum_{n=0}^{\infty} \epsilon^n \theta_n \quad \text{and} \quad q = \sum_{n=0}^{\infty} \epsilon^n q_n \tag{4.1}$$

into (3.1*a*) and (3.1*b*) yields at $O(1)$,

$$\theta_0 = 0 \quad \text{on } w \in \mathbb{R}^+, \tag{4.2}$$

$$q_0 = \left(\frac{w}{w+1}\right)^{\sigma}. \tag{4.3}$$

Then at $O(\epsilon)$, (3.1*a*) and (3.1*b*) yield

$$\theta_1 = -q_0^2 \frac{\mathrm{d}q_0}{\mathrm{d}w}, \tag{4.4}$$

$$\frac{q_1}{q_0} + \mathrm{i}\theta_1 = \mathscr{H}[\theta_1(w)]. \tag{4.5}$$

The full expressions for the higher $O(\epsilon^n)$ terms are more complicated, but since we are only concerned with the limit $n \to \infty$, we may proceed as follows: examine the leading-order free surface, $q_0(w)$ in (4.3); the solution contains two singularities, identifiable with points in the flow domain – one at the corner of the stern ($w = -1$) and the other at the stagnation point ($w = 0$). However, because all the higher-order problems are linear, no new singularities can be introduced and thus the singular points of $q_n(w)$ must be the same singularities as for $q_0(w)$.

For example, if we examine the dynamic condition in (3.1*b*), we can see that each successive term of the asymptotic approximation will require the derivative of the previous term. Thus if q_n contains a singularity of the form $1/(w - w_0)^n$, q_{n+1} will contain a singularity of the form $n/(w - w_0)^{n+1}$; each new derivative adds a factor to the numerator and increases the strength of the singularity. Then as $n \to \infty$, we can

expect the late-order terms to behave like factorial over power,

$$\theta_n \sim \frac{\Theta(w)\Gamma(n+\gamma)}{\chi(w)^{n+\gamma}} \quad \text{and} \quad q_n \sim \frac{Q(w)\Gamma(n+\gamma)}{\chi(w)^{n+\gamma}}. \tag{4.6}$$

With this ansatz in mind, we can now pinpoint the terms required at $O(\epsilon^n)$. In the limit that $n \to \infty$, terms like $q_m q_n$ (for m finite) dominate terms with smaller indices in n, such as $q_m q_{n-1}$. Moreover, differentiating a term increases the order (in n) by 1, so a term like $\epsilon\, \mathrm{d}q_{n-1}/\mathrm{d}w$ is of the same order as q_n. The relevant terms at $O(\epsilon^n)$ are

$$\overbrace{\frac{q_n}{q_0} + \mathrm{i}\theta_n}^{\text{first-order}} - \overbrace{\frac{q_{n-1}q_1}{q_0^2}}^{\text{second-order}} + \cdots = \overbrace{\mathscr{H}[\theta_n]}^{\text{exp. subdominant}}, \tag{4.7}$$

$$\underbrace{q_0^2 q_{n-1}'}_{\text{first-order}} + \underbrace{2q_0 q_1 q_{n-2}' + 2q_0 q_0' q_{n-1}}_{\text{second-order}} + \cdots = \underbrace{-\cos(\theta_0)\theta_n}_{\text{first-order}} + \cdots. \tag{4.8}$$

By recourse to Chapman & Vanden-Broeck (2006), we claim, at least for the moment, that the integral on the right-hand side of the boundary integral equation (4.7) is exponentially subdominant to the terms on the left-hand side for large n. We address this claim a little later in § 5.3, but for now, we will assume that

$$\theta_n \sim \mathrm{i}\frac{q_n}{q_0} - \frac{\mathrm{i}q_1 q_{n-1}}{q_0^2} + \cdots \quad \text{as } n \to \infty, \tag{4.9}$$

or

$$q_n \sim -\mathrm{i}q_0\theta_n - \mathrm{i}\theta_{n-1}q_1 + \cdots \quad \text{as } n \to \infty. \tag{4.10}$$

Finally, substituting (4.9) into the dynamic condition (4.8) and simplifying yields the final form of our $O(\epsilon^n)$ expression:

$$\overbrace{[q_0^3 q_{n-1}' + \mathrm{i}q_n]}^{\text{first/second-order}} + \underbrace{\left[2q_0^2 q_0' q_{n-1} + 2q_0^2 q_1 q_{n-2}' - \mathrm{i}\frac{q_{n-1}q_1}{q_0}\right]}_{\text{second-order}} + \cdots = 0. \tag{4.11}$$

The factorial-over-power ansatz (4.6) can now be substituted into (4.11). As $n \to \infty$, the leading-order expression is

$$-q_0^3\frac{\mathrm{d}\chi}{\mathrm{d}w} + \mathrm{i} = 0, \tag{4.12}$$

which is simply solved to yield

$$\chi = \int^w \frac{\mathrm{i}}{q_0^3(\varphi)}\,\mathrm{d}\varphi, \tag{4.13}$$

where we will choose the initial point of integration in the next section. At the next order in n, we find

$$Q' q_0^3 + 2Qq_0^2 q_0' - 2Qq_0^2 q_1\chi' - \mathrm{i}Q\frac{q_1}{q_0} = 0 \tag{4.14}$$

or, using (4.12) and simplifying,

$$\frac{Q'}{Q} = -\frac{2q_0'}{q_0} + \frac{3\mathrm{i}q_1}{q_0^4}. \tag{4.15}$$

Thus by integration and simplification, we have

$$Q = \frac{\Lambda}{q_0^2} \exp\left(3\mathrm{i}\int_{w^\star}^{w} \frac{q_1(\varphi)}{q_0^4(\varphi)}\,\mathrm{d}\varphi\right), \tag{4.16}$$

where Λ is a constant of integration and $w^\star$ is any arbitrary point for which the integral exists. By the ansatz (4.6) and relation (4.9), we know that $\theta_n \sim \mathrm{i}q_n/q_0$ and thus

$$\Theta = \frac{\Lambda\mathrm{i}}{q_0^3} \exp\left(3\mathrm{i}\int_{w^\star}^{w} \frac{q_1(\varphi)}{q_0^4(\varphi)}\,\mathrm{d}\varphi\right). \tag{4.17}$$

5. The singulant and its Stokes lines

In this section, we will use the expression (4.13) for the singulant, χ, to address three separate questions: (*a*) Must the stagnation point at the origin produce an exponentially small wave on the free surface? (*b*) What necessary conditions are imposed on the corner of the hull in order for it to generate a wave? (*c*) How can the boundary integral on the right-hand side of (3.1*a*) be shown to be exponentially subdominant to the residue contributions on the left?

5.1. *The stagnation point*

The nature of the free surface near the stagnation point, $w = 0$, is a surprisingly complex problem. First, there is the issue of how the solution behaves near $w = 0$ at a fixed value of ϵ (the inner problem); the works of, for example, Dagan & Tulin (1972) and Vanden-Broeck & Tuck (1994) have examined some of these problems. Second, there is the question of how the solution near $w = 0$ interacts with the low-Froude-number expansion of (4.1) and in particular, what is its role (if any) in controlling the production of downstream waves. In regard to this latter question, Tuck (1991*a*) has provided a series of unanswered questions for simpler differential equations related to the full water wave equations in (3.1*a*) and (3.1*b*).

The local analysis near the stagnation point for ϵ fixed and $w \to 0$ is given in Appendix A. There we show that

$$q = \begin{cases} O(w^\sigma) & \text{if } \sigma \geqslant 1/3 \\ O(w^{1/3}) & \text{if } \sigma < 1/3 \end{cases} \tag{5.1}$$

and

$$\theta = \hat{\theta}_0 + O(w^\kappa) = \begin{cases} 0 + O(w^{3\sigma-1}) & \text{if } \sigma \geqslant 1/3 \\ \pi\left(\sigma - \frac{1}{3}\right) + O(w^\varsigma) & \text{if } \sigma < 1/3, \end{cases} \tag{5.2}$$

where ς is a transcendental number given by solving (A 13), and $\hat{\theta}_0$ and κ are introduced for later use. Thus, equation (5.2) states that for hulls with $\sigma \geqslant 1/3$, the near-stagnation flow is the same as the rigid-wall solution; but for hulls with $\sigma < 1/3$, the free surface makes a $2\pi/3$ angle with the ship – very much like the cusp of a highest Stokes wave (Wehausen & Laitone 1960).

Now we investigate the inner limit of the outer approximations. Consider first (4.5):

$$q_1 = -\mathrm{i}q_0\theta_1 + \frac{q_0}{\pi}\int_0^\infty \frac{\theta_1(\varphi)}{\varphi - w}\,\mathrm{d}\varphi. \tag{5.3}$$

In the case of $1/3 < \sigma < 1$, the integrand satisfies the Hölder condition on the interval $[0, \infty)$ and moreover, $\theta_1(0) = 0$. This guarantees that

$$\frac{1}{\pi}\int_0^\infty \frac{\theta_1(\varphi)}{\varphi - w}\,\mathrm{d}\varphi \sim \frac{1}{\pi}\int_0^\infty \frac{\theta_1(\varphi)}{\varphi}\,\mathrm{d}\varphi = \text{constant} \tag{5.4}$$

as $w \to 0$. Thus $q_1 \sim q_0$ as $w \to 0$ (the residue contribution $-\mathrm{i}q_0\theta_1$ is lower order) and by induction $q_n \sim q_{n-1}$ for all n. In other words, for hulls with $\sigma > 1/3$, the singular nature of the origin does not magnify as n increases and hence there is no eventual divergence in the asymptotic series. In this case, then, there is no exponential contribution.

Now consider the case $0 < \sigma < 1/3$. Here, the outer solution behaves like $q_0 = O(w^\sigma)$ and consequently $\theta_1 = O(w^{3\sigma-1})$ tends to infinity at the stagnation point. An inner layer is required where the solution has the behaviour of (A 14) as $w \to 0$. In any case, we can write

$$\mathscr{H}[\theta_1(w)] = \frac{-\sigma}{\pi}\int_0^\infty \frac{\mathrm{d}\varphi}{\varphi^{1-3\sigma}(\varphi - w)} + \frac{\sigma}{\pi}\int_0^\infty \frac{-(\varphi+1)^{-1-3\sigma}+1}{\varphi^{1-3\sigma}(\varphi - w)}\,\mathrm{d}\varphi. \tag{5.5}$$

It is easy to verify that the rightmost integrand satisfies the Hölder condition on $[0, \infty)$ and is thus bounded and tending to a definite limit as $w \to 0$. The integral on the left contains a power singularity and thus by (Gakhov 1990, p. 55), $\mathscr{H}[\theta_1(w)] = O(w^{3\sigma-1})$. Inductively continuing this line of reasoning verifies that the growth of the integral term is indeed proportional to the growth of the residue term and thus

$$q_n = O(\mathrm{i}q_0\theta_{n-1}) \quad \text{as } n \to \infty. \tag{5.6}$$

This shows that for $\sigma \leqslant 1/3$, the singularity does cause the late-order outer terms to diverge and, moreover, at a rate specified by the ansatz (4.6). Thus, the stagnation point must be accompanied by the Stokes Phenomenon and the switching-on of exponentials. Still, it is entirely possible that the accompanying Stokes line does not come to intersect the free surface (other than at $w = 0$) and/or lies on a separate Riemann sheet altogether; *this is our conjecture*. And while the claim remains unproven, the numerical analysis of the problem in § 7 provides compelling evidence in its favour. We will return to this issue in the discussion of § 8.

5.2. *The corner*

The corner is the critical point which is responsible for the generation of waves. Since $\chi(-1) = 0$, we may write (4.13) as

$$\chi = \mathrm{i}\int_{-1}^{w} \frac{1}{q_0^3(\varphi)}\,\mathrm{d}\varphi = \mathrm{i}\int_{-1}^{w}\left(\frac{\varphi+1}{\varphi}\right)^{3\sigma}\mathrm{d}\varphi, \tag{5.7}$$

where the contour of integration can be taken along any path in the upper half-plane that does not go through $w = 0$. In fact, this expression can be exactly integrated in terms of special functions, and

$$\chi(w) = -\mathrm{i}(-w)^{3\sigma}w^{-3\sigma}B(-w;\, 1-3\sigma,\, 1+3\sigma) + 3\sigma\pi\left[1 + \mathrm{i}\cot(3\sigma\pi)\right], \tag{5.8}$$

where $B(x, y)$ is the Beta function. Near the corner,

$$q_0 \sim \mathrm{e}^{\pi\mathrm{i}\sigma}(w+1)^{-\sigma} \quad \text{and} \quad \chi \sim \left[\frac{\mathrm{i}\mathrm{e}^{-3\pi\mathrm{i}\sigma}}{1+3\sigma}\right](w+1)^{1+3\sigma} \tag{5.9}$$

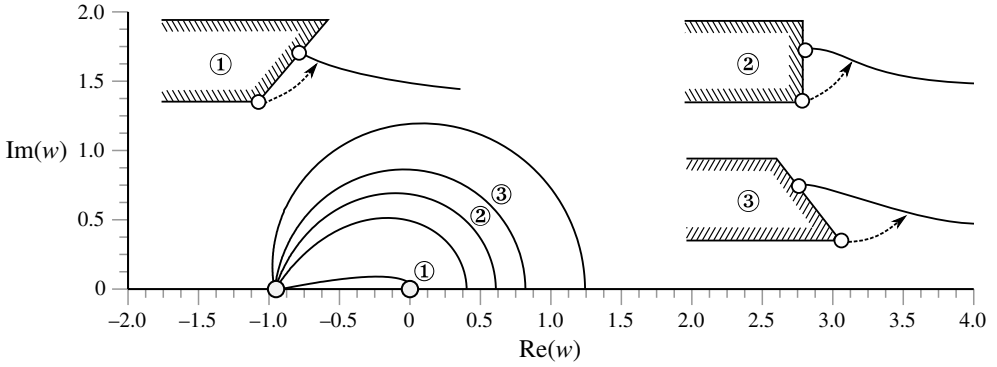

FIGURE 4. Stokes lines for various hulls: $\sigma = 0.2$ ①, $\sigma = 0.4$, $\sigma = 0.5$ ② , $\sigma = 0.6$ ③, and $\sigma = 0.8$. The Stokes lines are closed loops that begin and end at $w = -1$ and are symmetrical about the real axis. Across the intersection of the Stokes line with $\mathrm{Re}(w) > 0$, we expect an exponential to switch on. Although they are an imaginary construct and lie on the analytically continued free surface, they nevertheless share a correspondence with a line in the physical plane which begins at the corner and arcs towards the free surface.

and from Dingle (1973), Stokes lines are expected whenever $1 + 3\sigma > 0$, and also

$$\mathrm{Im}(\chi) = 0 \quad \text{and} \quad \mathrm{Re}(\chi) \geqslant 0. \tag{5.10}$$

The first (and only relevant) Stokes line leaves the critical point at an angle of

$$\vartheta = \pi \left(\frac{3\sigma - 1/2}{1 + 3\sigma} \right), \tag{5.11}$$

arcs into the upper half-plane, and continues until it intersects the free surface. This is shown in figure 4. We note that as $\sigma \to 0$, the intersection point tends towards the origin. In § 6 and onwards, we will focus what happens when each Stokes line is crossed.

5.3. *Exponential subdominance of the integral*

In order to demonstrate the late-order subdominance of the boundary integral in (3.1*a*), consider the case of $\sigma = 1/2$ (other values of σ are treated similarly). Here, the Stokes line originating from the corner leaves at an angle of $2\pi/5$ in the potential plane, curves in an arc, and intersects the free surface at about $w = \phi_c \approx 0.635$. Along the real and positive w-axis, $\mathrm{Re}(\chi) = 3\pi/2$, which can be computed by the residue contribution of (5.7) at infinity or alternatively by using (5.8).

In figure 5, we plot the contours of $|\chi(w)|$, a thick line representing the Stokes line, as well as a dashed line for the contour $|\chi| = 3\pi/2$. Since $\chi(w)$ is an analytic function away from its singularities, the contour $|\chi| = 3\pi/2$ must necessarily intersect both the Stokes line and the real axis at the single point $w = \phi_c$. Moreover, along the real axis the point ϕ_c constitutes an absolute minimum. For the equation

$$\frac{q_n}{q_0} + \mathrm{i}\theta_n - \frac{q_{n-1}q_1}{q_0^2} + \cdots = \mathscr{H}[\theta_n(w)], \tag{5.12}$$

when the ansatz (4.6) is used and the late terms sought, the integral will be evaluated on the real axis, where χ is larger than anywhere along the Stokes line. Thus the right-hand side of the equation is negligible as $n \to \infty$. Essentially, its only effect is in altering the values of the early terms, q_0, q_1, q_2, and so on.

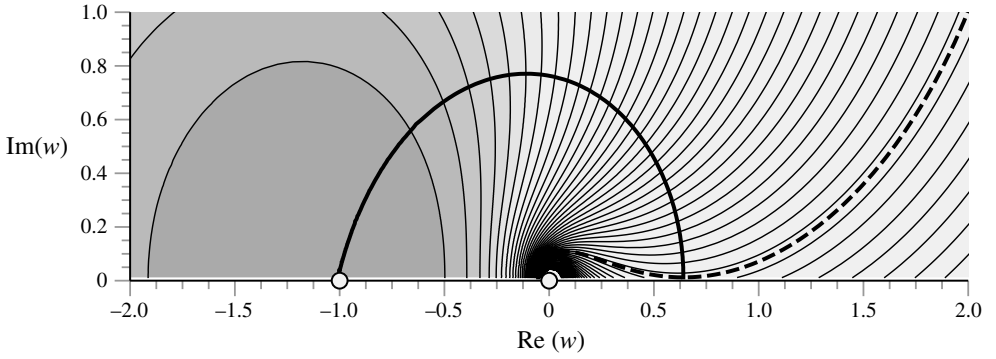

FIGURE 5. The thin lines are contours for $|\chi(w)|$, with dark regions corresponding to small values. The thick black line corresponds to the Stokes line, and the dashed line to $|\chi(w)| = 3\pi/2$. Our Stokes line switching analysis is confined to the region above the dashed line, where the relevant exponentials are larger than anywhere along the free surface.

The subdominance of the boundary integral term which occurs in potential theory was also used for the analysis of the viscous fingering problem in Hele-Shaw flows (see for example Combescot *et al.* 1988; Chapman 1999) and was rigorously justified for that problem by Xie & Tanveer (2002).

6. Inner problem

In the previous sections, we derived the general form of the high-order terms q_n and θ_n, up to the determination of certain unknown coefficients, namely Λ and γ. In this section, we will show how these coefficients can be determined by matching the high-order terms near the singularities in the flow field.

6.1. *Inner limits of outer expansions*

Before we begin studying the inner problem, let us take note of the behaviour of Q and Θ as we tend towards to the flow field singularity, $w = -1$. Recall from (4.16) and (4.17) that

$$Q = \frac{\Lambda}{q_0^2}\exp\left(3\mathrm{i}\int_{w^\star}^{w}\frac{q_1(\varphi)}{q_0^4(\varphi)}\,\mathrm{d}\varphi\right) \quad \text{and} \quad \Theta = \frac{\Lambda\mathrm{i}}{q_0^3}\exp\left(3\mathrm{i}\int_{w^\star}^{w}\frac{q_1(\varphi)}{q_0^4(\varphi)}\,\mathrm{d}\varphi\right), \tag{6.1}$$

while from (4.5), q_1 is given by

$$q_1 = -\mathrm{i}q_0\theta_1 + q_0\mathscr{H}[\theta_1(w)]. \tag{6.2}$$

Using $\theta_1 = -q_0^2\,\mathrm{d}q_0/\mathrm{d}w$ from (4.4), we have

$$q_1 = \mathrm{i}q_0^3\frac{\mathrm{d}q_0}{\mathrm{d}w} + q_0\mathscr{H}[\theta_1(w)]. \tag{6.3}$$

Thus the exponential factor in the expressions for Q and Θ in (6.1) can be written as

$$\begin{aligned}\exp\left(3\mathrm{i}\int_{w^\star}^{w}\frac{q_1(\varphi)}{q_0^4(\varphi)}\,\mathrm{d}\varphi\right) &= \exp\left(-3\int_{w^\star}^{w}\frac{q_0'(\varphi)}{q_0(\varphi)}\,\mathrm{d}\varphi\right)\exp\left(3\mathrm{i}\int_{w^\star}^{w}\frac{\mathscr{H}[\theta_1(\varphi)]}{q_0^3(\varphi)}\,\mathrm{d}\varphi\right)\\ &= \frac{q_0^3(w^\star)}{q_0^3(w)}\exp\left(3\mathrm{i}\int_{w^\star}^{w}\frac{\mathscr{H}[\theta_1(\varphi)]}{q_0^3(\varphi)}\,\mathrm{d}\varphi\right).\end{aligned} \tag{6.4}$$

For this equation, the integrand is well behaved near the singularity at $w=-1$ and so

$$\exp\left(3\mathrm{i}\int_{w^\star}^{w}\frac{q_1(\varphi)}{q_0^4(\varphi)}\,\mathrm{d}\varphi\right)\sim\frac{C}{q_0^3(w)}, \tag{6.5}$$

where C is the constant

$$C=q_0^3(w^\star)\exp\left(3\mathrm{i}\int_{w^\star}^{-1}\frac{\mathscr{H}[\theta_1(\varphi)]}{q_0^3(\varphi)}\,\mathrm{d}\varphi\right), \tag{6.6}$$

and thus the inner limits of the late-order terms of the outer expansion are

$$\theta_n\sim\frac{\mathrm{i}\Lambda C}{q_0^6}\frac{\Gamma(n+\gamma)}{\chi^{n+\gamma}}\quad\text{and}\quad q_n\sim\frac{\Lambda C}{q_0^5}\frac{\Gamma(n+\gamma)}{\chi^{n+\gamma}}. \tag{6.7}$$

The values of C for various hulls are computed in Appendix B. In order to select the constant γ, we require the asymptotic behaviour of the late terms given in (4.6), to be consistent with the order of the singularities of q_0 and θ_0 as $w\to-1$. Equating powers, we need $-5\sigma-(1+3\sigma)\gamma=\sigma$ or

$$\gamma=\frac{6\sigma}{1+3\sigma}, \tag{6.8}$$

which is equivalent to (3.22) in Chapman & Vanden-Broeck (2006).

6.2. *Outer limit of inner expansions*

Let us begin by discussing how the two governing equations change as we tend towards the corner. Near the singularity, the dynamic condition (3.1*b*) remains unchanged, but the boundary integral (3.1*a*) can be considerably simplified. In this case, we would like to evaluate

$$\log q_{inner}(w)+\mathrm{i}\theta_{inner}(w)=\mathscr{H}[\theta_{outer}(w)] \tag{6.9}$$

as $w\to-1$ and where the indices help to remind us where the functions q and θ are being evaluated. The left-hand side is evaluated near the singularity and thus involves the exact expressions for $q(w)$ and $\theta(w)$ in the inner limit. However, the integrand on the right-hand side is integrated over the free surface, far away from the singularity, thus it involves only the outer expansion for $\theta(w)$. But we know that substituting the outer expansion into the right-hand side of (6.9) leads to

$$\log q_{inner}(w)+\mathrm{i}\theta_{inner}(w)=\log q_0+\epsilon\mathscr{H}[\theta_1(w)]+O(\epsilon^2), \tag{6.10}$$

and since $\mathscr{H}[\theta]$ is well-behaved for w off the axis, this forms a well-ordered asymptotic expansion. The leading-order inner solution, then, is equivalent to using $\log q+\mathrm{i}\theta\sim\log q_0$ and we may thus substitute

$$\sin\theta=\frac{\mathrm{e}^{\mathrm{i}\theta}-\mathrm{e}^{-\mathrm{i}\theta}}{2\mathrm{i}}\sim\frac{\mathrm{i}}{2}\left(\frac{q}{q_0}-\frac{q_0}{q}\right) \tag{6.11}$$

into the dynamic condition (3.1*b*), yielding

$$\epsilon q_0 q^3\frac{\mathrm{d}q}{\mathrm{d}w}+\frac{\mathrm{i}}{2}\left(q^2-q_0^2\right)=0. \tag{6.12}$$

The correct scaling to use is hinted at by the inner limits of the outer approximations. In the inner region, where $q_0\sim c(w+1)^{-\sigma}$ with $c=\mathrm{e}^{\pi\mathrm{i}\sigma}$, we let

$$w=-1+\epsilon^{1/1+3\sigma}\eta\quad\text{and}\quad q=c\mathrm{e}^{-\sigma/(1+3\sigma)}\eta^{-\sigma}\overline{q}. \tag{6.13}$$

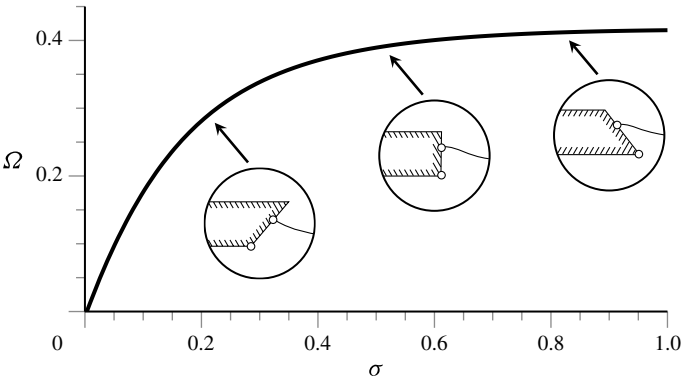

FIGURE 6. Values of Ω, from (6.17), for various hull forms.

Then (6.12) becomes

$$2\mathrm{i}c^3\overline{q}^2\left(-\sigma\eta^{-3\sigma-1}\overline{q}+\eta^{-3\sigma}\frac{\mathrm{d}\overline{q}}{\mathrm{d}\eta}\right)=\overline{q}-\frac{1}{\overline{q}}. \tag{6.14}$$

We now let

$$z=\frac{\mathrm{i}\eta^{1+3\sigma}}{c^2(1+3\sigma)},\quad \phi=\overline{q}^2\quad\text{and}\quad \phi=\sum_{n=0}^{\infty}\frac{\phi_n}{z^n}, \tag{6.15}$$

yielding a recurrence relation for the outer limit of the leading-order inner solution:

$$\phi_0=1,\quad \phi_n=\sum_{m=0}^{n-1}\left(m+\frac{2\sigma}{1+3\sigma}\right)\phi_m\phi_{n-m-1}, \tag{6.16}$$

valid for $z\to\infty$. We match the leading-order inner limit of the nth term of the outer expansion of q^2 and match with the outer limit of the nth term of the leading-order inner expansion. Using (5.9), (6.7), (6.13) and (6.15) gives

$$\Lambda=\frac{c^{6-3\gamma}\mathrm{e}^{\mathrm{i}\pi\gamma/2}}{2C(1+3\sigma)}\underbrace{\lim_{n\to\infty}\frac{\phi_n}{\Gamma(n+\gamma)}}_{\Omega}. \tag{6.17}$$

The crucial limiting ratio, Ω, only depends on the local power of the singularity, and numerical values for different ships are given figure 6. Notice that Ω is strictly positive for all positive positive values of σ. In the next section, we will explain how this fact relates to the production of waves.

6.3. *Stokes smoothing*

Remember: the underlying divergence of the asymptotic expansions will cause the *Stokes Phenomenon* to occur, and as the complexified asymptotic solution crosses a critical curve (the *Stokes line*), a small exponential switches on. The details of the Stokes smoothing procedure are precisely the same as in Chapman & Vanden-Broeck (2006), and here, we will only summarize the key ideas.

In order to identify the exponentially small waves, we first optimally truncate the asymptotic series at $n = \mathscr{N}$ so that

$$\theta = \sum_{n=0}^{\mathscr{N}} \epsilon^n \theta_n + R_{\mathscr{N}} \quad \text{and} \quad q = \sum_{n=0}^{\mathscr{N}} \epsilon^n q_n + S_{\mathscr{N}}, \tag{6.18}$$

whereby the remainders are related by (4.9) and thus $S_{\mathscr{N}} \sim -\mathrm{i}q_0 R_{\mathscr{N}}$. At the optimal truncation point, the remainder $S_{\mathscr{N}}$ is exponentially small (rather than only algebraically small) and can be written as $S_{\mathscr{N}}(w) = \mathscr{S}(w) Q \mathrm{e}^{-\chi/\epsilon}$, where we expect $\mathscr{S}(w)$ to smoothly vary from zero to a constant across the Stokes line.

The procedure then is to re-scale near the Stokes line and examine the jump in the exponentially small remainder as the Stokes line is crossed from upstream (indicated with a + below) to downstream (indicated with a − below). The apparent jump in the remainder of q can be shown to be

$$\left[S_{\mathscr{N}}\right]_+^- \sim \frac{2\pi\mathrm{i}}{\epsilon^\gamma} Q \mathrm{e}^{-\chi/\epsilon}, \tag{6.19}$$

while for θ, the jump is

$$\left[R_{\mathscr{N}}\right]_+^- \sim \frac{2\pi\mathrm{i}}{\epsilon^\gamma} \Theta \mathrm{e}^{-\chi/\epsilon}. \tag{6.20}$$

To finalise the analysis, we also need to complexify the free boundary into the lower half-plane and this analogous process yields the functional complex conjugates of (6.19) and (6.20); thus, the total contribution along the free surface is twice the real parts of (6.19) and (6.20),

$$q_{exp} \sim \frac{4\pi}{\epsilon^\gamma} \mathrm{Im}(Q \mathrm{e}^{-\chi/\epsilon}), \tag{6.21}$$

$$\theta_{exp} \sim \frac{4\pi}{\epsilon^\gamma} \mathrm{Im}(\Theta \mathrm{e}^{-\chi/\epsilon}). \tag{6.22}$$

These formulae provide a link between the terms that are switched on across Stokes lines, and the late-order terms of the asymptotic series.

6.4. *The simplified nonlinear problem*

The attentive reader will have noticed that the only effect of the Hilbert transform, $\mathscr{H}[\theta(w)]$, is to adjust the far-field waves by a non-zero constant factor. In fact, if we were to simply ignore $\mathscr{H}[\theta]$, the only effects would be: (i) changing q_1 in (4.5), (ii) changing the computation of C in (6.6), and (iii) replacing the expression of Q in (4.16), valid everywhere, by its expression valid near the singularity.

Thus, the salient features of the problem can still be retained if we use $\log q \pm \mathrm{i}\theta = \log q_0$ instead of (3.1*a*), and in this way, we can reduce the full problem in (3.1*a*) and (3.1*b*) to a simpler nonlinear differential equation in q. Analytic continuation into the upper half-plane then gives the simpler formulation:

$$\epsilon q_0 q^3 \frac{\mathrm{d}q}{\mathrm{d}w} + \frac{\mathrm{i}}{2}\left(q^2 - q_0^2\right) = 0. \tag{6.23}$$

Tuck (1991*a*) also realised that the essential characteristics of the waveless ship problem could be encapsulated by a single, local differential equation (his example, however, was pedagogic in nature, whereas our approximation is justifiable). The

one-cornered ship problem can thus be analysed more simply by studying (6.23) instead of the full problem, and this is briefly presented in Trinh, Chapman & Vanden-Broeck (2010); in fact, we shall use this simplified formulation to study the more difficult multi-cornered ship problem in a future paper.

However, we now return to our study of the full problem in (3.1*a*) and (3.1*b*), for which we have already completed the asymptotic analysis. In the next section, we will provide numerical validation of our beyond-all-orders predictions.

7. Numerical results

Precise computation of exponential smallness is hardly a trivial affair, but despite the fact that the quantities of interest are exceedingly small, many past workers have still managed to confirm *beyond-all-orders* predictions with numerical simulations. For example, by using a spectral basis supplemented by a function which mimics the far-field waves, Boyd (1991) was able to compute the exponentially small gravity–capillary waves of the fifth-order Korteweg–de Vries equation to over ten digits of accuracy. And although these methods were never applied to the full nonlinear water-wave equations, Chapman & Vanden-Broeck (2002, 2006) still comfortably computed small capillary and small gravity waves for the full problem using second-order finite differences – this time to five or six digits of accuracy. Unfortunately, as we shall see, the ship–wave problem presents numerous new challenges not encompassed by the previous numerical methods. These challenges arise because of the surface-piercing nature of the ship, which supplements the usual difficulties of resolving exponential smallness with the problem of now dealing with an essential singularity at the origin.

We shall present two algorithms for resolving the far-field waves in the limit of small Froude number. ALGORITHM A is quick and simple, and can be used whenever ϵ is not too small or when the effect of the singularity is minimal. When either of these two conditions is violated, we opt for ALGORITHM B, which uses a stretched grid near the singularity. Both approaches were necessary to achieve our results, but we emphasise the rather severe sensitivity of the waves (at small ϵ) to particular parameter choices of the two algorithms; because of this, we have taken great care to ensure reproducibility of all our results. The numerical difficulties encountered in this paper have inspired recent work by Olver (2011) on developing spectral methods for solving Riemann–Hilbert problems.

7.1. *ALGORITHM A: a simple method*

We first propose a very simple method based on the work in Chapman & Vanden-Broeck (2002, 2006), though many authors have used this method for computing two-dimensional nonlinear flows over obstructions (see for example Forbes 1983 for the case of gravity flow over a semi-circular cylinder, and King & Bloor 1990 for the case of flow over an arbitrary bed topography).

To begin, we first truncate the semi-infinite domain to a finite interval and introduce an equally spaced mesh for ϕ and its midpoints, with separation distance, $\Delta\phi$:

$$\phi_j = (j-1)\Delta\phi \quad \text{for } j = 1, 2, \ldots, n, \tag{7.1}$$

$$\phi_j^m = \tfrac{1}{2}(\phi_j + \phi_{j+1}) \quad \text{for } j = 1, 2, \ldots, n-1. \tag{7.2}$$

We seek to solve for the n unknowns, θ_j (evaluated at the points ϕ_j). Given an initial guess for θ_j, values of $\tau = \log q$ at the $n-1$ midpoints are computed using

$$\tau_j^m = \sigma \log\left(\frac{\phi_j^m}{\phi_j^m + 1}\right) + \frac{1}{\pi} \fint_{-3pt0}^{\phi_{max}} \frac{\theta(\phi)}{\phi - \phi_j^m} \, \mathrm{d}\phi \quad \text{for } j = 1, 2, \ldots, n-1. \tag{7.3}$$

The principal value integral is computed by applying the trapezoidal rule with a summation over the mesh points ϕ_j; this use of equally spaced points and midpoints should allow us to neglect the singularity of the principal value without losing accuracy. Bernoulli's equation then provides a system of $n-1$ equations to solve:

$$F_j = \epsilon \mathrm{e}^{3\tau_j^m} \left(\frac{\mathrm{d}\tau^m}{\mathrm{d}\phi_m}\right)_j + \sin\theta_j^m = 0 \quad \text{for } j = 1, 2, \ldots, n-1, \tag{7.4}$$

where the derivatives $\mathrm{d}\tau/\mathrm{d}\phi$ are computed using second-order differences, and θ_j^m denotes the value of θ at the midpoints. For the nth equation, we assign the boundary condition

$$F_n = \theta_1 = \begin{cases} 0 & \text{if } \sigma \geqslant \frac{1}{3} \\ \pi(\sigma - \frac{1}{3}) & \text{if } \sigma < \frac{1}{3}, \end{cases} \tag{7.5}$$

and moreover, we replace the first equation with the condition that

$$F_1 = \theta_3 - \hat{\theta}_0 - (\theta_2 - \hat{\theta}_0)\left(\frac{\phi_3}{\phi_2}\right)^{\kappa} = \theta_3 - \hat{\theta}_0 - (\theta_2 - \hat{\theta}_0)2^{\kappa}, \tag{7.6}$$

where $\hat{\theta}_0$ and κ are as prescribed in (5.2). Conditions (7.5) and (7.6) then assure us that $\theta = \hat{\theta}_0 + O(\phi^{\kappa})$ over the first three mesh points.

Solutions for the $\sigma = 20/48$ and $\sigma = 32/48$ hulls at $\epsilon = 0.8$ and $\epsilon = 0.4$, respectively are shown in figure 7. It is important to note that the values shown are not from θ_j but rather, the midpoints θ_j^m; this is due to the fact that the central difference approach in the algorithm causes the original θ values to exhibit a sawtooth pattern between mesh points – it is, after all, the midpoints which are used in the solution of (7.4). Notice from the enlarged lower figure that even for these relatively moderate values of ϵ, the downstream waves are already quite small. The algorithm is most effective for both moderate values of σ (near or greater than the vertical hull) and moderate wave amplitudes. Unfortunately, it proves to be ineffective for specific types of solutions, due to certain numerical difficulties, as we shall now discuss.

The first difficulty is that the method of computing singular integrals by trapezoidal integration over the midpoints is generally not as accurate as other comparable second-order methods, particularly when the singularity is allowed to approach one of the endpoints (see Noble & Beighton 1980). For increased accuracy, we need an alternative treatment of the boundary integral.

The second minor difficulty is that compared to the amplitude of the far-field waves, the algebraic decay of the core solution is extremely slow, at the rate of

$$\theta = O\left(\frac{w^{3\sigma-1}}{(w+1)^{3\sigma+1}}\right), \tag{7.7}$$

as $\epsilon \to 0$ and $w \to \infty$. Wave amplitudes are measured by computing differences in numerical maxima and minima near ϕ_{max}, and increased accuracy can be achieved by averaging the small, locally linear shifts in the amplitudes. However, this slow algebraic decay is a symptom of the surface-piercing nature of the problem and still

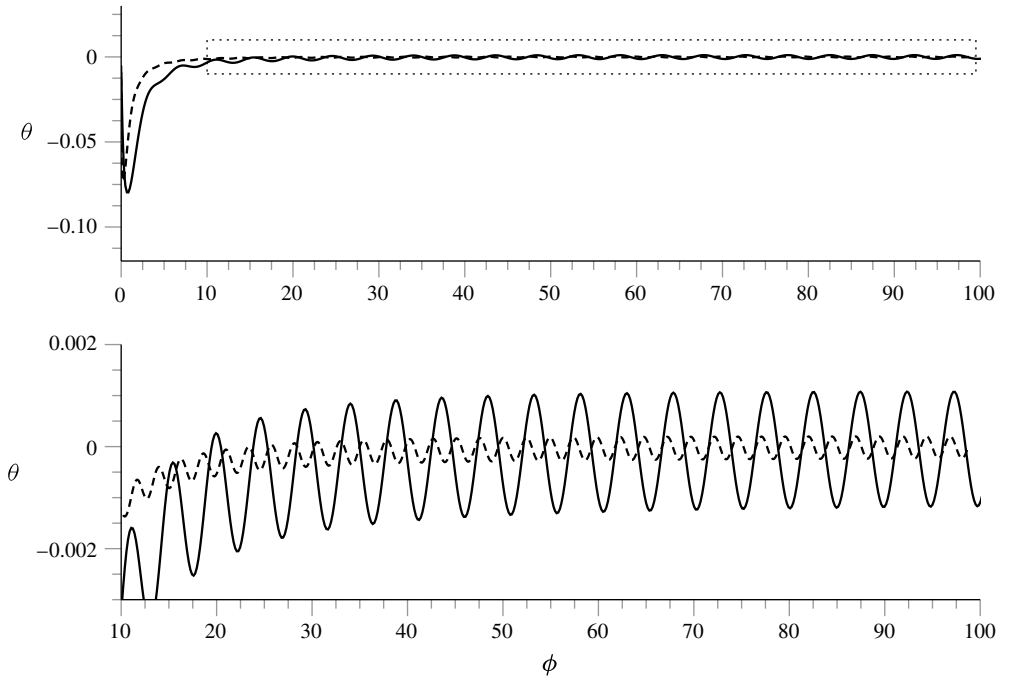

FIGURE 7. Solutions for $\sigma = 20/48$ at $\epsilon = 0.4$ (dashed) and $\sigma = 32/48$ at $\epsilon = 0.8$ (solid); these solutions were computed using ALGORITHM A with $n = 2000$ and $\Delta\phi = 0.05$ for the former hull, and $n = 1000$ and $\Delta\phi = 0.1$ for the latter. Zooming in (not shown) shows that the solution is ill-resolved near the stagnation point, but for a limited range of hulls, the algorithm is sufficient.

provides an additional loss of accuracy in comparison with problems for which the tails are generally exponentially decaying – as in the fifth-order Korteweg–de Vries problem discussed in Boyd (1991), and also for gravity flows over a submerged obstruction studied in Chapman & Vanden-Broeck (2006).

Finally and most importantly, for values of σ near or less than $1/3$, the algorithm does a poor job of approximating the solution, particularly those containing wave amplitudes on the order of 10^{-3}. Examination of θ near the stagnation point shows that the numerical discretisation cannot cope with the essential singularity at the origin; unfortunately, as $\sigma \to 0$, the outer low-Froude-number solution becomes increasingly singular. The inherent errors in using an inappropriately spaced mesh swamp the computations and low-Froude-number solutions for σ small cannot be trusted.

In the next section, we will propose an alternative algorithm which focuses on minimising the errors produced by the stagnation point.

7.2. *ALGORITHM B: a comprehensive method*

The algorithm in this section is similar to the one presented in Farrow & Tuck (1995) but with a few key differences which allow a better resolution of the near-stagnation flow.

The first change we implement is the use of a stretched grid in ϕ near the stagnation point. We need a mesh which can approximate the essential singularity at the origin, but which can also capture the almost-periodic waves downstream. For this, we define

a stretched grid near the origin

$$\phi_j = \phi_0 + (\phi_c - \phi_0)\left(\frac{j-1}{m-1}\right)^{1/s} \quad \text{for } j = 1, 2, \ldots, m, \tag{7.8}$$

for some initial point ϕ_0, some *matchpoint* ϕ_c, a chosen number of mesh points m, and a value of s we will later specify. Afterwards, a downstream discretisation is chosen:

$$\phi_j = \phi_c + \Delta\phi_{max}\left(\frac{j-1}{n-m-1}\right) \quad \text{for } j = m+1, 2, \ldots, n, \tag{7.9}$$

for a total of n mesh points and a downstream spacing of $\Delta\phi_{max}$. A better parameter to use for the latter is given by

$$K = \frac{2\pi\epsilon}{\Delta\phi_{max}}, \tag{7.10}$$

where K now indicates the number of mesh points per linear wavelength of the downstream waves. If the value of s is not too small, then we may select ϕ_c and m so that the last separation distance of the initial mesh, $\phi_m - \phi_{m-1}$, is equal to the spacing of the downstream mesh, $\Delta\phi_{max}$; we refer to this as a *smoothed mesh*. However, if s is too small, then the growth of the initial mesh is too slow, and we generally need to manually choose suitable values of ϕ_c and m for each individual problem. The complete choice of parameters which fully determine the initial and downstream mesh is quite tricky and largely dependent on the choice of σ and ϵ. For solutions given in the figures, we let $\boldsymbol{B}(\sigma) = [n, \phi_0, K, m, \phi_c]$ denote a vector of parameter values, and write $\boldsymbol{B}(\sigma) = [n, \phi_0, K, *, *]$ if a *smoothed mesh* is used. In the next section, however, we will discuss which particular values work and which do not.

Here, we look to solve

$$F_j = \frac{\epsilon}{3}q_0^3(\phi_j)\exp\left[\frac{1}{\pi}\fint_{\phi_1}^{\phi_n}\frac{\theta(\varphi)}{\varphi-\phi_j}\,\mathrm{d}\varphi\right] + \int_{\phi_1}^{\phi_j}\sin\theta\,\mathrm{d}\varphi = 0, \tag{7.11}$$

for $j = 1, 2, \ldots, n$, and the principle advantage of dealing with (7.11) rather than its differentiated counterpart, (7.4), is that the lack of smoothness between the two meshes at $\phi = c$ can now be ignored.

Now we turn to the computation of the right-most integral. We proceed as in Farrow & Tuck (1995), and split the integral as

$$\int_0^{\phi_j}\sin\theta\,\mathrm{d}\varphi = \int_0^{\phi_{j-1}}\sin\theta\,\mathrm{d}\varphi + \int_{\phi_{j-1}}^{\phi_j}\sin\theta\,\mathrm{d}\varphi. \tag{7.12}$$

The second integral on the right is calculated by computing the quadratic interpolation of $\sin\theta$ over ϕ_{j-1}, ϕ_j and ϕ_{j+1}, and integrating the quadratic exactly (the use of the additional ϕ_{j+1} point is to ensure stability and accuracy of the method). Similarly, for the integral

$$\fint_0^{\infty}\frac{\theta(\varphi)}{\varphi-\phi_j}\,\mathrm{d}\varphi = \int_0^{\phi_{j-1}}\frac{\theta(\varphi)}{\varphi-\phi_j}\,\mathrm{d}\varphi + \fint_{\phi_{j-1}}^{\phi_{j+1}}\frac{\theta(\varphi)}{\varphi-\phi_j}\,\mathrm{d}\varphi + \int_{\phi_{j+1}}^{\phi_{max}}\frac{\theta(\varphi)}{\varphi-\phi_j}\,\mathrm{d}\varphi, \tag{7.13}$$

the first and last terms on the right-hand side can be computed using the trapezoid rule, whereas the singular term is calculated by fitting a quadratic through the points θ_{j-1}, θ_j, and θ_{j+1} and integrating exactly.

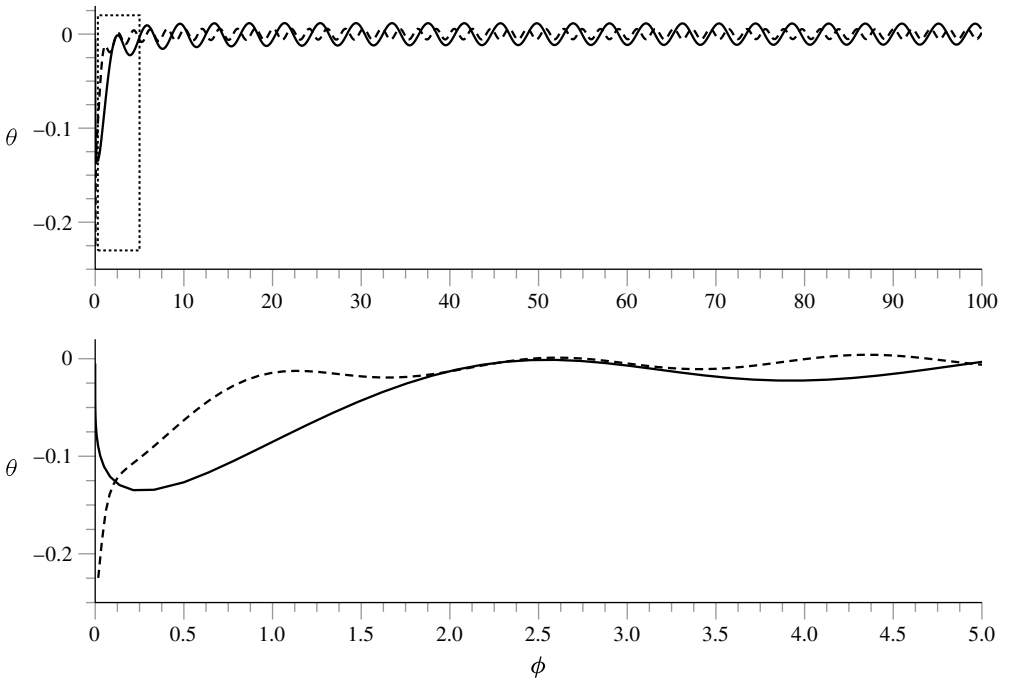

FIGURE 8. Solutions for $\sigma = 12/48$ at $\epsilon = 1/3$ (dashed) and $\sigma = 18/48$ at $\epsilon = 1/3$ (solid). These were computed using the stretched grids of ALGORITHM B and as shown in the enlargement in the lower figure, successfully produced well-resolved solutions near the stagnation point. Parameters used were: $\boldsymbol{B}(12/48) = [1450, 10^{-8}, 30, 20, 0.5]$ and $\boldsymbol{B}(18/48) = [800, 10^{-8}, 30, 20, 0.5]$.

Next, let us turn to boundary conditions. The selection of the number and type of boundary conditions to impose is generally an *ad hoc* issue. In general, we must worry about the solution remaining bounded at the last endpoint $\phi = \phi_{max}$, and moreover, for it to have the correct behaviour as $\phi \to 0$. For the former condition, we find it sufficient to construct a quadratic interpolation through the three next-to-last mesh points, and require the last mesh point to satisfy this relation; that is,

$$F_n = \theta_n - (p_2\phi_n^2 + p_1\phi_n + p_0) = 0, \tag{7.14}$$

where p_0, p_1 and p_2 are the coefficients of the quadratic satisfying $p_2\phi_j^2 + p_1\phi_j + p_0 = \theta_j$ for $j = n-3, n-2$ and $n-1$.

The behavioural condition as $\phi \to 0$ is more difficult. For example, we could simply ignore the issue, and assume that our choice for the near-field discretisation would be sufficient for the solution to converge. Alternatively, we could impose the condition that the quadratically extrapolated value from the first three mesh points coincides with the correct value of θ at the origin. That is,

$$F_1 = \hat{\theta}_0 - (p_2\phi_1^2 + p_1\phi_1 + p_0) = 0, \tag{7.15}$$

where $\hat{\theta}_0$ is from (5.2), and p_2, p_1 and p_0 are the coefficients of the quadratic which satisfy $p_2\phi_j^2 + p_1\phi_j + p_0 = \theta_j$, for $j = 1, 2$ and 3.

Another condition could be to require that

$$F_1 = \theta_2 - \theta_1 \left(\frac{\phi_2}{\phi_1} \right)^{\kappa} = 0, \tag{7.16}$$

where κ is as prescribed in (5.2). Other possibilities may be to require that $q(0) = 0$ using a condition akin to (7.15); or perhaps, to require that $q = O(w^{\sigma})$ if $\sigma \geqslant 1/3$ and $q = O(w^{1/3})$ if $\sigma < 1/3$ using a condition akin to (7.16).

As a general rule of thumb, the conditions in (7.15) and (7.16) both seem adequate and more-or-less equivalent in correctly resolving the behaviour near the stagnation point, provided the mesh is suitably chosen. With this in mind, we choose to use (7.15) as this does not require κ. Examples of successfully computed solutions are given in figure 8.

7.3. *Numerical versus analytical results*

In the end however, even with various *ad hoc* changes to accommodate the numerical challenges of the surface-piercing and singular-integral aspects of the problem, it is still difficult to understand how one change may affect the resultant wave amplitudes in contrast with another. Because our regime of interest involves exponentially small waves, small changes in not only the choice of boundary conditions, but also the number of mesh points to place in the both the initial and downstream mesh can have a significant impact on the eventual results.

We leave these questions concerning the construction of a truly robust and accurate numerical method for further research and instead focus on sufficient confirmation of our analytical results. Our numerical results are constructed by relying on a combination of all the techniques mentioned in the previous sections.

In general, there are five crucial parameters to choose when using ALGORITHM B. These are n, the total number of mesh points; m, the number of points in the stretched grid; ϕ_0, the first grid point; ϕ_c, the matchpoint between the two meshes; and finally K, the points per wavelength. For small ϵ, a small adjustment to one of these parameters can have a significant impact on the relative error of the solutions.

Let us begin with the easiest case: the $\sigma = 1/2$ hull is simplest to calculate because its waves are only moderately small, and its behaviour near the origin only moderately singular. Here, ALGORITHM A provides accurate results for amplitudes down to roughly 10^{-4}. Afterwards, the more careful treatment of the stagnation point and quadrature schemes from ALGORITHM B can be used to extend these results down to around 10^{-6}.

There is a surprising requirement for numerical accuracy of hulls with σ larger than $1/2$. For these cases, the behaviour near the stagnation point is less singular and, in fact, the increase in accuracy gained from ALGORITHM B over A is less significant. However, for smaller and smaller wave amplitudes, it becomes crucial to increase the number of points per wavelength; in the case of $\sigma = 5/8$, for example, accurate results can only be obtained for $\epsilon \approx 0.5$ with $K = 60$–90 points per wavelength. With this in mind, both algorithms provide similar results, and because the simpler version is much more computationally efficient, we favour it for these larger values of σ.

The most challenging regime occurs when σ is small and particularly when $\sigma < 1/3$. In this case, it is crucial to correctly resolve the behaviour near the stagnation point. Here, the difficulty is that the solution exhibits two types of behaviour near the critical point: as ϵ tends to zero, the outer solution tends to negative infinity at the rate of $\theta \sim w^{3\sigma-1}$, which is a particularly strong blow-up. However, the nonlinear inner region

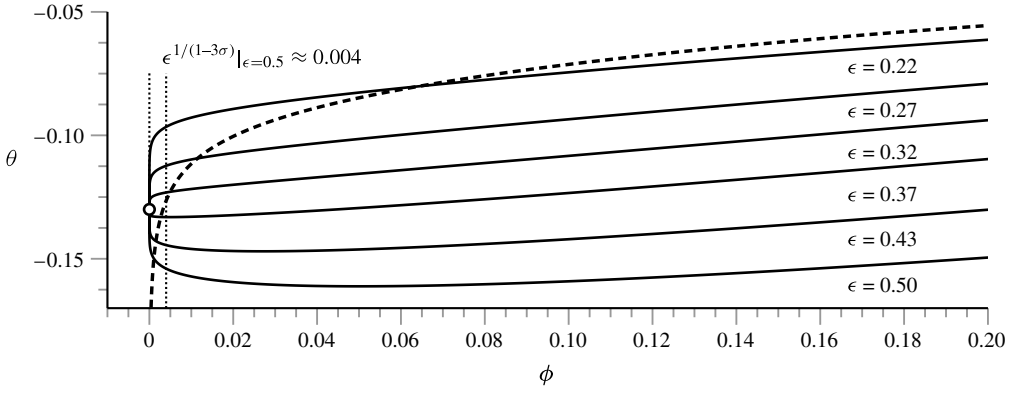

FIGURE 9. Solutions near the stagnation point for $\sigma = 14/48$ and for various values of ϵ. The leading-order asymptotic solution for $\epsilon = 0.22$ is the dashed line whereas the small node indicates the value $\theta_0 \approx -0.13$. Initially (for $\epsilon = 0.5$), there is a fairly clear inner region (marked on the figure). As $\epsilon \to 0$, this inner region grows smaller and smaller, making it increasingly difficult to resolve the inner-most solution. All computations used $\boldsymbol{B}(14/48) = [1000, 10^{-8}, 30, *, *]$.

has $\theta \sim \theta_0 + w^{\varsigma}$, which behaves almost linearly for small σ (see (5.2) in § 5.1). Worst still, the inner region is growing ever smaller and smaller, at the rate of $\epsilon^{1/1-3\sigma}$.

Consider the case of $\sigma = 14/48 \approx 0.2917$. In this problem, the outer solution roughly behaves like $\theta \sim w^{-0.13}$, whereas the nonlinear prediction is $\theta = \theta_0 + w^{0.39}$. These two behaviours are not wholly disparate. In this case, we may use ALGORITHM B with the choice of $s = \varsigma \approx 0.39$ for the initial mesh. The choice is then sufficiently singular to resolve the correct near-field behaviour and provide accurate results for wave amplitudes down to about 10^{-6}. Figure 9 is a blow-up of the stagnation point for solutions of this ship for various values of ϵ.

Now consider the most challenging case: for $\sigma = 12/48 = 0.25$, the outer solution roughly behaves like $\theta \sim w^{-0.25}$, whereas the nonlinear prediction is $\theta = \theta_0 + w^{0.89}$. Choosing s from either approximation leads to trouble. Our *ad hoc* solution has been to choose a value of s sufficiently small to resolve the outer blow-up, but within reach of the true nonlinear behaviour – for example $s = 0.25$. Once solutions for this mesh have been computed, we may then slowly increase s while increasing m and examine the convergence of the solutions.

By patiently adjusting each of the values involved in the computations, we have been able to construct figure 10, which plots numerical and asymptotic results for the hulls we have discussed, accurate to around five or six digits of accuracy. The slopes of the semi-log trends are each matched to a particular hull, with the backward-facing hulls ($\sigma > 1/2$) producing smaller waves than the forward-facing hulls. The agreement between analytical and numerical results is very good, even over relatively large ranges of ϵ.

8. Discussion

So in the end, do *waveless ships exist*?

For the one-cornered ship, the answer is clearly no. The Stokes line smoothing necessitates the existence of the non-zero wave on the free surface. For stern flows, these waves must propagate downstream, while for bow flows, these waves grow to

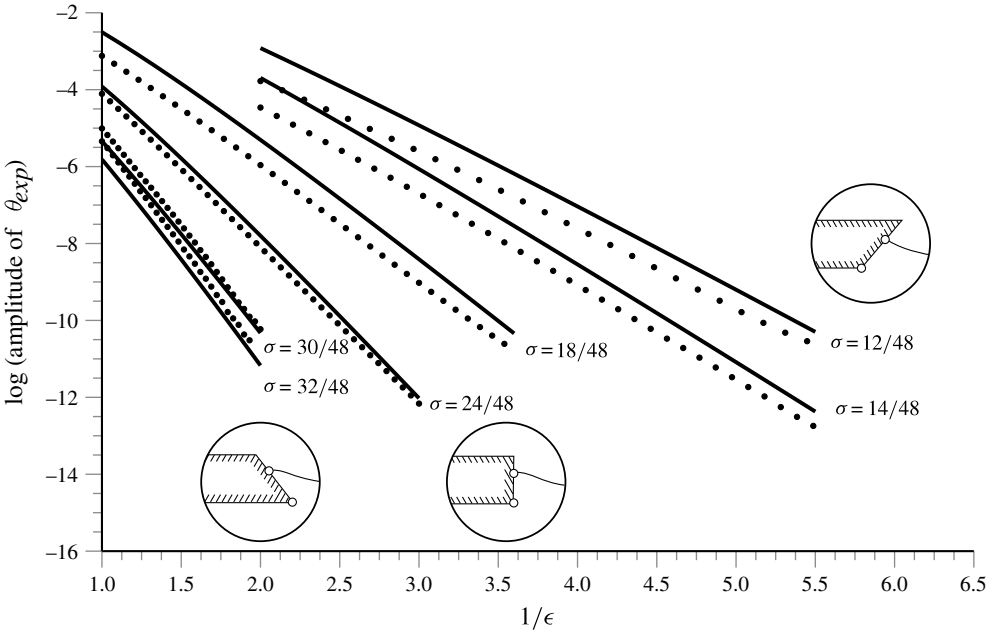

FIGURE 10. Numerical (dots) and asymptotic (solid) wave amplitudes in θ, far downstream and for a range of hull inclinations. At a given Froude number, the waves can be minimised by simply inclining the hull 'backwards'. The asymptotic predictions from (6.22) provide a good fit for a large range of Froude numbers. The $\sigma = 32/48$ computation was done using ALGORITHM A with $n = 1500$ and discretisation distance $\Delta\phi = 0.04$; similarly, the $\sigma = 30/48$ computation used $n = 1500$ and $\Delta\phi = 0.05$; the rest were done using ALGORITHM B. The following parameter values were used: $\boldsymbol{B}(12/48) = [800, 10^{-8}, 30, 90, 0.3]$, $\boldsymbol{B}(14/48) = [1000, 10^{-8}, 30, *, *]$, $\boldsymbol{B}(18/48) = [800, 10^{-8}, 30, 50, 0.5]$, and $\boldsymbol{B}(24/48) = [800, 10^{-5}, 30, 20, 0.5]$.

be of infinite amplitude near the hull (since $|Q|, |\Theta| \to \infty$ as $w \to 0$ in (6.1)). In particular, this implies that for such flows, the assumption that the flow attaches to the hull at a stagnation point is false; indeed, it has been conjectured that the correct assumption must include an overturning splash near the bow (see Dias & Vanden-Broeck 1993; Tuck 1994). Thus for the one-cornered hull, neither waveless sterns nor splashless bows are possible.

But there are still a handful of open questions, and many of these unresolved issues are significant for the wider study of general free-surface problems. One such issue, which we had previously encountered in § 5.1, deals with the attachment between free surface and ship when the inclination of the hull is less than $\pi/3$; here, does the stagnation point produce an exponentially small contribution on the surface? Our numerics seem to indicate that it does not, but this issue of *evanescent* waves near a free-surface singularity has already been highlighted as a particularly challenging problem (see Tuck 1991*a*,*b*), and we invite other researchers to address the issue.

Another open issue relates to the separation of our mathematical analysis into local and global approaches. For example, consider the late-order terms of § 4, or consider the local emergence of the Stokes lines of § 5.2, or the numerical solution of the recurrence relation of § 6; all these results were derived using local properties of the problem – indeed, their analysis simply depends on the behaviour of the asymptotic

solutions near the relevant singularities. In contrast, the global nature of the ship problem, which largely depends on the physical set-up, must be handled on a case-by-case basis. Are there less obvious Stokes line arrangements, not examined in this study, which produce different classes of solutions?

In discussing these global issues, we are naturally led to the following question: *Do waveless ships of a more general form exist?* Perhaps. One could imagine that for a general multi-cornered ship (such as the one depicted as ② in figure 1) the position of each corner could be strategically chosen so that the wave contribution due to each singularity adds to zero in the far field – the entire body would then move without a wake. In a future paper, we shall demonstrate that for most 'obvious' classes of multi-cornered ships, total wave cancellation does not occur. Moreover, it seems to be the case that the bulbous ships studied by Tuck & Vanden-Broeck (1984) (shown as ③ in figure 1) cannot be made waveless either; indeed, this was the claim in Farrow & Tuck (1995) based on numerical evidence. Research on this problem is ongoing.

Appendix A. Local behaviour near the stagnation point

In this appendix, we will derive the local behaviour of the free surface near the stagnation point along the ship's hull. For the local behaviour, it is initially easier to work with Cartesian coordinates as a function of the potential $z = z(w)$, and now, assuring analyticity of z (or w) is equivalent to satisfying the boundary integral equation; we may thus focus on Bernoulli's equation (2.3), which can be written as

$$-\frac{2}{\epsilon}\mathrm{Im}[z]\left|\frac{\mathrm{d}z}{\mathrm{d}w}\right|^2 = 1 \quad \text{on } w \in \mathbb{R}^+, \tag{A 1}$$

where the wall condition requires that

$$\sin(\pi\sigma)\left(\frac{\mathrm{d}x}{\mathrm{d}w}\right) - \cos(\pi\sigma)\left(\frac{\mathrm{d}y}{\mathrm{d}w}\right) = 0 \quad \text{on } w \in (-1, 0). \tag{A 2}$$

Now, one way to proceed is to let

$$z(w) \sim \mathscr{A} w^\alpha + \mathscr{B} w^\beta \tag{A 3}$$

where $\mathscr{A}, \mathscr{B} \in \mathbb{C}$ and we are concerned with $w \to 0$. Tuck & Roberts (1997) instead consider $z = X(w) + \mathrm{i}Y(w)$ where they require $X, Y \in \mathbb{R}$ on $w \in \mathbb{R}^+$, but the two approaches are equivalent. We now have to split everything into real and imaginary parts and multiply out. If we write

$$z = [a\mathrm{e}^{\mathrm{i}\delta}]w^\alpha + [b\mathrm{e}^{\mathrm{i}\rho}]w^\beta, \tag{A 4}$$

where $\beta > \alpha$, and all the variables save for w are real, then we find two possible cases. First, if $\delta = 0$, then the requirement that z is real on $w \in \mathbb{R}^+$ is satisfied automatically, whereas the wall condition in (A 2) requires that $\alpha = 1 - \sigma$. Thus,

$$z(w) \sim a w^{1-\sigma} \Rightarrow \frac{\mathrm{d}w}{\mathrm{d}z} = q\mathrm{e}^{-\mathrm{i}\theta} \sim \mathscr{C} w^\sigma, \tag{A 5}$$

where the constants $\mathscr{C}$ and a cannot be determined purely by local means. The expression in (A 5) is simply the leading-order solution in the small-ϵ limit.

Now suppose on the other hand that $\delta \neq 0$. Then we may write

$$\frac{\mathrm{d}z}{\mathrm{d}w} = \hat{\mathscr{A}}\mathrm{e}^{\mathrm{i}\delta} w^{\alpha-1} + \hat{\mathscr{B}}\mathrm{e}^{\mathrm{i}\rho} w^{\beta-1}, \tag{A 6}$$

where we have denoted $\hat{\mathscr{A}} = \alpha a$ and $\hat{\mathscr{B}} = \beta b$. Then along the free surface, we can write for $w = \phi > 0$,

$$\left|\frac{\mathrm{d}z}{\mathrm{d}w}\right|^2 = \hat{\mathscr{A}}^2\phi^{2\alpha-2} + \hat{\mathscr{B}}^2\phi^{2\beta-2} + 2\hat{\mathscr{A}}\hat{\mathscr{B}}\cos(\delta-\rho)\phi^{\alpha+\beta-2}, \tag{A 7}$$

whereas

$$\mathrm{Im}(z) = \mathrm{Im}[a\mathrm{e}^{\mathrm{i}\delta}\phi^{\alpha} + b\mathrm{e}^{\mathrm{i}\rho}\phi^{\beta}] = [a\sin\delta]\phi^{\alpha} + [b\sin\rho]\phi^{\beta}. \tag{A 8}$$

We may now write the free-surface condition in (A 1) as

$$[a\sin(\delta)\phi^{\alpha} + b\sin(\rho)\phi^{\beta}][\hat{\mathscr{A}}^2\phi^{2\alpha-2} + \hat{\mathscr{B}}^2\phi^{2\beta-2} + 2\hat{\mathscr{A}}\hat{\mathscr{B}}\cos(\delta-\rho)\phi^{\alpha+\beta-2}] = \frac{\epsilon}{2}. \tag{A 9}$$

The leading-order dominant balance requires

$$a^3\alpha^2\sin(\delta)\phi^{3\alpha-2} = -\frac{\epsilon}{2}, \tag{A 10}$$

so $\alpha = 2/3$ and the wall condition in (A 2) requires $\delta = \pi\sigma - \pi/3$. Finally, a can be determined by substituting these values into (A 10), yielding

$$a = \left[\frac{9\epsilon}{8\sin(\pi/3 - \pi\sigma)}\right]^{1/3}. \tag{A 11}$$

The next order in the free-surface equation is $\phi^{2\alpha+\beta-2}$, where

$$2\beta\sin(\pi\sigma - \pi/3)\cos(\pi\sigma - \pi/3 - \rho) + (2/3)\sin\rho = 0, \tag{A 12}$$

and here, the wall condition requires that $\rho = \pi\sigma - \pi\beta - 1$; substituting this into the above gives

$$2\beta\sin(\pi\sigma - \pi/3)\cos(2\pi/3 + \pi\beta) + 2/3\sin(\pi\sigma - \pi\beta - 1) = 0. \tag{A 13}$$

The above expression provides a formula for the transcendental power, β and in fact it can be shown that the series expansion for $z(w)$ with ϵ fixed and $w \to 0$ proceeds in transcendental powers after the first term. Nevertheless, along the free surface, we may write

$$\theta = \delta + \left(\frac{b}{a}\right)\phi^{\beta-\alpha}\left\{\frac{\sin\rho}{\cos\delta} - \tan(\delta)\frac{\cos\rho}{\cos\delta}\right\} + O\left(\phi^{2\beta-2\alpha}\right) = \delta + \mathscr{D}\phi^{\varsigma}, \tag{A 14}$$

where we define the important power as $\varsigma = \beta - \alpha = \beta - 2/3$ and the constant $\mathscr{D}$ cannot be found by local means alone.

Appendix B. Computation of C in (6.6)

In this appendix, we will analytically derive $|C|$ and provide numerical computations for the argument of C. Without loss of generality, we will choose the initial point of integration $\varphi = w^{\star}$ to lie on the positive real axis. There is a residue contribution at $\varphi = \infty$, so we will also let $\zeta' = 1/\varphi$. The integral becomes

$$C = q_0^3(w^{\star})\exp\left(-3\mathrm{i}\int_{1/w^{\star}}^{w^{*}}\frac{1}{\zeta'^2 q_0^3(1/\zeta')}\left[\frac{1}{\pi}\int_0^{\infty}\frac{\theta_1(t)}{t - 1/\zeta'}\,\mathrm{d}t\right]\mathrm{d}\zeta'\right), \tag{B 1}$$

where the singularity is $w^\star = -1$ for the one-cornered ship. Now since we are only interested in the modulus of C, we note that for real ζ',

$$\operatorname{Im}\left[\frac{1}{\pi}\int_0^\infty \frac{\theta_1(t)}{t-1/\zeta'}\,\mathrm{d}t\right] = \begin{cases} 0, & \zeta' < 0 \\ \theta_1, & \zeta' > 0 \end{cases} \tag{B 2}$$

the residue being positive since we wish to remain in the upper half-φ-plane during integration. Thus

$$\begin{aligned} &\operatorname{Re}\left(-3\mathrm{i}\int_{1/w^\star}^{w^*} \frac{1}{\zeta'^2 q_0^3(1/\zeta')}\left[\frac{1}{\pi}\int_0^\infty \frac{\theta_1(t)}{t-1/\zeta'}\,\mathrm{d}t\right]\mathrm{d}\zeta'\right) \\ &\quad = 3\int_{1/w^\star}^{0} \frac{\theta_1(1/\zeta')}{\zeta'^2 q_0^3(1/\zeta')}\,\mathrm{d}\zeta' - 3\,\operatorname{Res}\left\{\frac{\dfrac{1}{q_0^3}\displaystyle\int_0^\infty \dfrac{\theta_1(t)}{t-1/\zeta'}\,\mathrm{d}t}{\zeta'^2}, \zeta'=0\right\}. \end{aligned} \tag{B 3}$$

Setting $\theta_1 = -q_0^2\,\mathrm{d}q_0/\mathrm{d}w$ by (4.5) and changing the first integral back to the w-plane yields

$$3\int_{w^\star}^\infty \frac{\theta_1(\varphi)}{q_0^3(\varphi)}\,\mathrm{d}\varphi = 3\int_{w^\star}^\infty \frac{q_0'(\varphi)}{q_0(\varphi)}\,\mathrm{d}\varphi = -3\log q_0(w^\star), \tag{B 4}$$

and the residue is

$$\operatorname{Res}\left\{\frac{\dfrac{1}{q_0^3}\displaystyle\int_0^\infty \dfrac{\theta_1(t)}{t-1/\zeta'}\,\mathrm{d}t}{\zeta'^2}, \zeta'=0\right\} = \operatorname{Res}\left\{\frac{\dfrac{1}{q_0^3}\displaystyle\int_0^\infty -\theta_1(t)\,\mathrm{d}t}{\zeta'}, \zeta'=0\right\} = \frac{1}{3}. \tag{B 5}$$

Thus

$$\operatorname{Re}\left(-3\mathrm{i}\int_{w^\star}^{-1} \frac{1}{q_0^3(\varphi)}\left[\frac{1}{\pi}\int_0^\infty \frac{\theta_1(t)}{t-\varphi}\,\mathrm{d}t\right]\mathrm{d}\varphi\right) = -3\log q_0(w^\star) - 1, \tag{B 6}$$

and so the magnitude of C is

$$|C| = \frac{1}{\mathrm{e}}. \tag{B 7}$$

Note that this computation for $|C|$ does not depend on the particular form of q_0, only that it tends to 1 as $w \to \infty$. The numerical computation of $\operatorname{Arg}(C)$ can be considerably simplified by using the exact expression for the inner integral,

$$\begin{aligned} \frac{1}{\pi}\int_0^\infty \frac{\theta_1(\varphi)}{\varphi - w}\,\mathrm{d}\varphi = \frac{\sigma}{3(1+w)}\Bigg[&\frac{1}{\sigma} + \frac{3\pi\exp(-3\pi\mathrm{i}\sigma)\operatorname{cosec}(3\sigma\pi)}{w}\left(\frac{w}{w+1}\right)^{3\sigma} \\ &+ \frac{3}{1-3\sigma}\,{}_2F_1(1, 1, 2-3\sigma, -w)\Bigg], \end{aligned} \tag{B 8}$$

where ${}_2F_1$ is the hypergeometric function. With this, (6.6) can now be computed by numerically integrating along a semi-circular arc in the upper half-plane from $w \in \mathbb{R}^+$ to $w = -1$. Figure 11 plots the values of $\operatorname{Arg}(C)$ for different hull configurations.

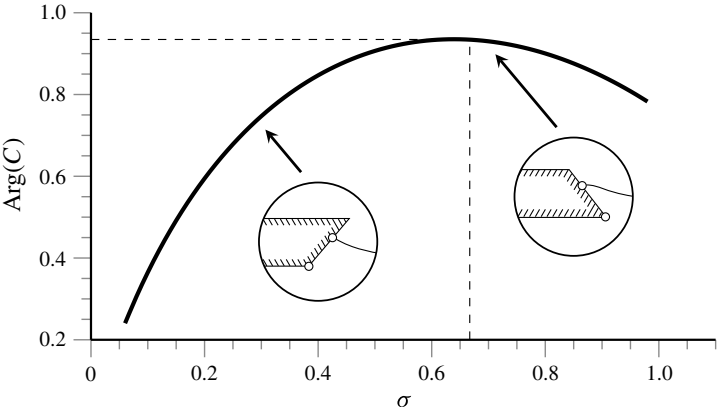

FIGURE 11. Numerically integrated values of Arg(C) for various hull forms. The argument reaches its maximum at $\sigma \approx 2/3$, where Arg(C) ≈ 0.9346.

REFERENCES

BABA, E. 1976 Wave breaking resistance of ships. In *Proc. Intl Seminar on Wave Resistance, Tokyo*, pp. 75–92.

BOYD, J. P. 1991 A comparison of numerical and analytical methods for the reduced wave equation with multiple spatial scales. *Appl. Numer. Maths* **7**, 453–479.

BOYD, J. P. 1998 *Weakly Nonlocal Solitary Waves and Beyond-All-Orders Asymptotics*. Kluwer.

BOYD, J. P. 1999 The Devil's invention: asymptotics, superasymptotics and hyperasymptotics. *Acta Appl.* **56**, 1–98.

CHAPMAN, S. J. 1999 On the role of Stokes lines in the selection of Saffman–Taylor fingers with small surface tension. *Eur. J. Appl. Maths* **10** (6), 513–534.

CHAPMAN, S. J. & VANDEN-BROECK, J.-M. 2002 Exponential asymptotics and capillary waves. *SIAM J. Appl. Maths* **62** (6), 1872–1898.

CHAPMAN, S. J. & VANDEN-BROECK, J.-M. 2006 Exponential asymptotics and gravity waves. *J. Fluid Mech.* **567**, 299–326.

COMBESCOT, R., HAKIM, V., DOMBRE, T., POMEAU, Y. & PUMIR, A. 1988 Analytic theory of the Saffman–Taylor fingers. *Phys. Rev.* A **37** (4), 1270–1283.

DAGAN, G. & TULIN, M. P. 1972 Two-dimensional free-surface gravity flow past blunt bodies. *J. Fluid Mech.* **51** (3), 529–543.

DIAS, F. & VANDEN-BROECK, J.-M. 1993 Nonlinear bow flows with spray. *J. Fluid Mech.* **255**, 91–102.

DINGLE, R. B. 1973 *Asymptotic Expansions: Their Derivation and Interpretation*. Academic.

FARROW, D. E. & TUCK, E. O. 1995 Further studies of stern wavemaking. *J. Austral. Math. Soc.* B **36**, 424–437.

FORBES, L. K. 1983 Free-surface flow over a semi-circular obstruction, including the influence of gravity and surface tension. *J. Fluid Mech.* **127**, 283–297.

GAKHOV, F. D. 1990 *Boundary Value Problems*. Dover.

KING, A. C. & BLOOR, M. I. G. 1990 Free-surface flow of a stream obstructed by an arbitrary bed topography. *Q. J. Mech. Appl. Maths* **43**, 87–106.

KOSTYUKOV, A. A. 1968 *Theory of Ship Waves and Wave Resistance*. Effective Communications Inc, (English translation).

KOTIK, J. & NEWMAN, D. J. 1964 A sequence of submerged dipole distributions whose wave resistance tends to zero. *J. Math. Mech.* **13**, 693–700.

MADURASINGHE, M. A. D. 1988 Splashless ship bows with stagnant attachment. *J. Ship Res.* **32** (3), 194–202.

MADURASINGHE, M. A. D. & TUCK, E. O. 1986 Ship bows with continuous and splashless flow attachment. *J. Austral. Math. Soc.* B **27**, 442–452.

NOBLE, B. & BEIGHTON, S. 1980 Error estimates for three methods of evaluating Cauchy principal value integrals. *J. Inst. Maths Applics* **26**, 431–446.

OGILVIE, T. F. 1968 Wave resistance: The low speed limit. *Tech Rep*. Michigan University, Ann Arbor.

OLVER, S. 2011 Computing the Hilbert transform and its inverse. *Maths Comput.* **80**, 1745–1767.

TRINH, P. H. 2010 Exponential asymptotics and free-surface flows. PhD thesis, University of Oxford.

TRINH, P. H., CHAPMAN, S. J. & VANDEN-BROECK, J.-M. 2010 The existence and non-existence of waveless ships. In *Proc. 25th Intl Workshop on Water Waves and Floating Bodies, Harbin, China, Harbin Engineering University*.

TUCK, E. O. 1991*a* Ship-hydrodynamic free-surface problems without waves. *J. Ship Res.* **35** (4), 277–287.

TUCK, E. O. 1991*b* Waveless solutions of wave equations. In *Proc. 6th International Workshop on Water Waves and Floating Bodies*. MIT.

TUCK, E. O. 1994 The planing splash. In *Proc. 9th Intl Workshop on Water Waves and Floating Bodies* (ed. M. Ohkusu). Kyushu University, Japan.

TUCK, E. O. & ROBERTS, A. J. 1997 Bow-like free surfaces under gravity. *Phil. Trans. R. Soc. Lond.* A **355**, 655–677.

TUCK, E. O. & VANDEN-BROECK, J.-M. 1984 Splashless bow flows in two-dimensions. In *Proc. 15th Symposium Naval Hydrodynamics*. National Academy Press.

TULIN, M. P. 2005 Reminiscences and reflections: ship waves, 1950–2000. *J. Ship Res.* **49** (4), 238–246.

VANDEN-BROECK, J.-M. 1980 Nonlinear stern waves. *J. Fluid Mech.* **96** (3), 603–611.

VANDEN-BROECK, J.-M. 1985 Nonlinear free-surface flows past two-dimensional bodies. In *Advances in Nonlinear Waves,* vol. 2, pp. 31–42. Pitman Publishing Inc.

VANDEN-BROECK, J.-M. 2010 *Gravity–Capillary Free-Surface Flows*. Cambridge University Press.

VANDEN-BROECK, J.-M. & TUCK, E. O. 1977 Computation of near-bow or stern flows using series expansion in the Froude number. In *2nd Intl Conf. on Numerical Ship Hydrodynamics, Berkeley, California*, University of California, Berkeley.

VANDEN-BROECK, J.-M. & TUCK, E. O. 1994 Flow near the intersection of a free surface with a vertical wall. *SIAM J. Appl. Maths* **54** (1), 1–13.

WEHAUSEN, J. V. & LAITONE, E. V. 1960 *Surface Waves*, *Encyclopedia of Physics*, IX. Springer.

XIE, X. & TANVEER, S. 2002 Analyticity and nonexistence of classical steady Hele–Shaw fingers. *Commun. Pure Appl. Maths* **56** (3), 353–402.

YEUNG, R. W. 1991 Nonlinear bow and stern waves – inviscid and viscous solutions. In *Mathematical Approaches in Hydrodynamics*, pp. 349–369. SIAM.